

Simulations of reflected radio signals from cosmic ray induced air showers

Jaime Alvarez-Muñiz^a Washington R. Carvalho Jr.^a
Daniel García-Fernández^a Harm Schoorlemmer^b Enrique Zas^a

^a*Departamento de Física de Partículas & Instituto Galego de Física de Altas
Energías,
Universidade de Santiago de Compostela, 15782 Santiago de Compostela, Spain*

^b*University of Hawaii at Manoa, Department of Physics and Astronomy,
Honolulu, Hawaii 96822, USA*

Abstract

We present the calculation of coherent radio pulses emitted by extensive air showers induced by ultra-high energy cosmic rays accounting for reflection on the Earth's surface. Results have been obtained with a simulation program that calculates the contributions from shower particles after reflection at a surface plane. The properties of the radiation are discussed in detail emphasizing the effects of reflection. The shape of the frequency spectrum is shown to be closely related to the angle of the observer with respect to shower axis, becoming hardest in the Cherenkov direction. The intensity of the flux at a fixed observation angle is shown to scale with the square of the primary particle energy to very good accuracy indicating the coherent aspect of the emission. The simulation methods of this paper provide the foundations for energy reconstruction of experiments looking at the Earth from balloons and satellites. They can also be used in dedicated studies of existing and future experimental proposals.

Key words: Cosmic Rays; Air Shower; Radio Detection;

Email addresses: Corresponding author: jaime.alvarezmuniz@gmail.com -
Phone: +34 881 813 968 - Fax: +34 881 814 086 (Jaime Alvarez-Muñiz),
carvajr@gmail.com (Washington R. Carvalho Jr.), sirzid@gmail.com (Daniel
García-Fernández), harmscho@phys.hawaii.edu (Harm Schoorlemmer),
zas@fpaxp1.usc.es (Enrique Zas).

1 Introduction

There is a renewed interest in using the radio technique for the detection of extensive air showers induced by Ultra-High Energy Cosmic Rays (UHECR). Dedicated experimental initiatives such as CODALEMA [1], LOFAR [2], AERA [3], LOPES [4] and Tunka-Rex [5], with instrumentation far superior to that used in the early days of radio detection, have stimulated an impressive progress in the field. As a result the possibility of using the radio technique, either as a complement to other techniques for the detection of extensive air showers, or even to design new UHECR detectors based on it, is now seriously considered [6].

The serendipitous discovery of 16 fast radio pulses from air showers extending up to the GHz range with the first ANITA balloon born antenna system [9] came as a surprise. This system, operating with a frequency band between 200 and 1200 MHz, had been originally conceived for detecting radio emission from neutrino interactions in the Antarctic ice sheet. However, the detected emission was strongly polarized in the direction defined by the cross product of the geomagnetic field and the shower direction, which is characteristic of radio signals from air showers due to the current induced by the Earth's magnetic field [1,10]. Detailed simulations of these pulses showed recently that coherent emission can extend up to and above GHz frequencies [7,8] in spite of simple dimensional arguments suggesting the contrary [12]. This is because the varying refractive index of the atmosphere introduces a significant effect on the relative travel time of emissions originating from different locations. When these delays are accounted for, a Cherenkov like ring can appear in which the signals from a large region of the shower arrive with little time delay and thus add coherently [8]. This angle is mostly determined by the refractive index at the shower maximum, simply because that is the region with more charge and current and hence contributing most.

Fourteen out of the sixteen detected pulses were reconstructed to be coming from distinct points on the polar ice cap and showed inverted polarity with respect to the other two. This was interpreted as clear evidence that they were detected after reflection on the polar ice cap. The reflection of the radio flashes introduces several new aspects to the calculation of pulses at the detector that have not been previously addressed. Naturally reflection implies a reduction of the emission due to the Fresnel coefficients. The relative time delays with respect to detection at ground level are also altered, since the pulses propagate upwards after reflection towards the top of the atmosphere along a decreasing refractive index profile. These effects need to be taken into consideration to interpret the events detected by ANITA and to evaluate the acceptance of experiments that rely on observing radiation induced by showers from mountain tops, balloon payloads [13] such as the next ANITA flight and EVA [14] or

from satellite payloads as proposed in SWORD [15].

In this article we simulate and describe the properties of radio pulses emitted from extensive air showers after reflection off a surface. Most of the calculations are performed in a configuration suited for a high altitude balloon flight over Antarctica, however the developed methods can be applied to other reflective surfaces and different detector altitudes. We modified the ZHAireS code [16] to calculate the radio emission from air showers after reflection on a flat surface. We first describe the geometry and explain the assumptions made to adapt the program to calculate the reflected radiation. After this we generate a set of simulations to investigate the signal properties as a function of off-axis angle, frequency, zenith angle, and energy of the primary particle, and stress the importance of properly accounting for the Fresnel coefficients in the reflection, as well as for the propagation of the pulses towards the top of the atmosphere. In the Appendix we use a ray tracing code and a simplified model for the emission (that displays the main features of the predicted radiation as has been justified elsewhere [8,17]), to confirm that the effect of curved light trajectories can be neglected.

2 Geometry and scales relevant for reflected events

The appealing aspect of observing radiation of air showers after reflection is that a large atmospheric volume can be monitored with a single detector. Therefore, the most interesting geometry is given by air showers that impact Earth's surface at large zenith angles. The basic geometry of the problem is sketched in Fig. 1. We define a rectangular coordinate system with the z -axis pointing upwards in the vertical direction and the $x - y$ plane tangent to the Earth's surface. The reflective surface will be approximated by this plane. The origin of the coordinate system is the point at which the shower axis intercepts the Earth's surface which is assumed to be at a ground altitude z_g above sea level. The zenith angle of the shower, θ , is defined with respect to the z -axis. We define the *off-axis angle* ψ in Fig. 2, to describe the angular deviation of the emitted radiation with respect to the shower axis¹. A generic detector is positioned at a point with vertical altitude h_d . In Fig. 1 the detector is displayed in a special position such that it sees the reflected radiation which was emitted precisely along the direction of shower axis with $\psi = 0^\circ$. The altitude at which shower maximum (X_{\max}) is reached, $h_{X_{\max}}$, is also of relevance. Besides determining the angle at which the emission is largest [8], it also sets the scale of distances the pulse has to travel to reach the detector, $d_{X_{\max}} + d_d$, where $d_{X_{\max}}$ and d_d respectively denote the distances from the origin of the

¹ ψ as depicted in Fig 2 is also used later in this work to refer to the location of the observer.

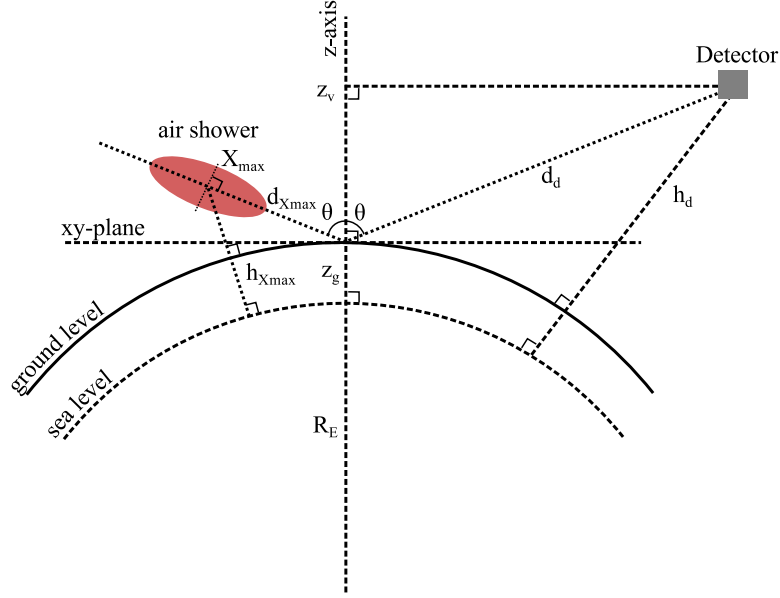


Fig. 1. Basic geometry for reflected signals from air showers (see text for details, see also Fig. 2).

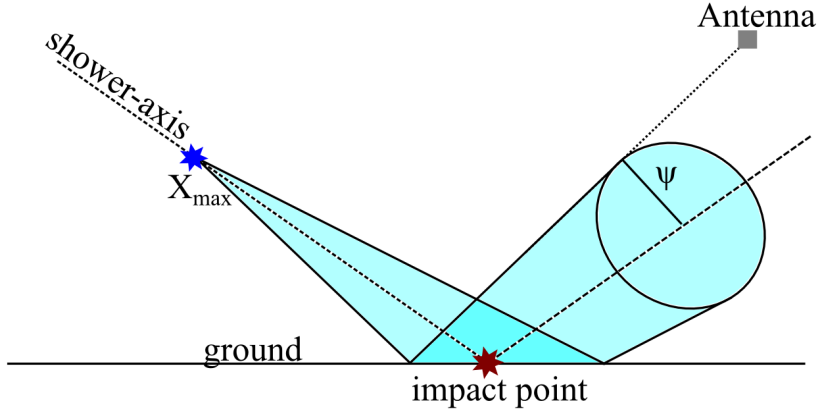


Fig. 2. To describe a location of an antenna we use the “off-axis” angle ψ , as that between the shower axis and the line joining the location of X_{\max} and the position of the antenna.

79 coordinate system to shower maximum and to the detector.

80 We illustrate the typical scales of this geometry by showing in Fig. 3 some
 81 parameters for a high altitude balloon over Antarctica. We take a detector
 82 at a typical altitude of $h_d = 35$ km, a ground altitude of the ice cap of $z_g =$
 83 2 km and the Earth’s radius $R_E = 6357$ km. The distance d_d becomes simply
 84 a function of θ which is illustrated in the top panel of Fig. 3. To estimate
 85 the distance to shower maximum, $d_{X_{\max}}$, we use the average slant depth of
 86 shower maximum $\langle X_{\max} \rangle$ as observed by the Pierre Auger Observatory [18,19]
 87 together with the atmospheric density profile used in the air shower simulation
 88 package AIRES [20]. Clearly the average position of X_{\max} depends on shower

energy, but the effect is accidentally small according to the measurements 89
at the Pierre Auger Observatory which indicate little change of X_{\max} in the 90
energy range of $10^{17.8}$ to $10^{19.6}$ [18,19]. The results for different primary energies 91
are shown as a function of θ in the middle panel of Fig. 3. It should be 92
noted that the measured RMS fluctuations of X_{\max} are between 20 and 60 93
 g cm^{-2} [18,19] corresponding to variations of $d_{X_{\max}}$ below 11% (3%) for a 94
zenith angle of 60° (85°) degrees. The variation relative to the total distance 95
travelled by the pulse $d_{X_{\max}} + d_d$ reduces to 1.5% (1.0%). 96

A relevant parameter is the Cherenkov angle, $\psi_C \approx \cos^{-1}(1/n)$, at the location 97
of X_{\max} that is directly obtained using the refractive index n at the correspond- 98
ing altitude, $h_{X_{\max}}$. In the following the refractive index is approximated by 99
a simple exponential function of altitude h given by $n(h) = 1 + \eta_0 e^{-\kappa h}$, with 100
 $\eta_0 = 325 \times 10^{-6}$ and $\kappa = 0.1218 \text{ km}^{-1}$ [16]. The Cherenkov angle at X_{\max} is 101
shown in Fig. 3 (bottom) for the above parameterization. 102

3 Introducing reflection in ZHAireS 103

ZHAireS [16] is a simulation program that has been developed combining 104
the AIRES package for air shower simulations [20] with the “ZHS algorithm” 105
which was originally developed to calculate radio emission from high energy 106
showers in homogeneous ice [21,22] and then extended for use in air show- 107
ers [16,23]. The contribution from each track element to the radio pulse at 108
any given position and time is calculated in ZHAireS assuming the particle 109
travels at a constant speed and in a rectilinear motion and also accounting for 110
the travel times taken by the radiation to reach from each of the ends of the 111
track [16,24]. To calculate travel times in ZHAireS we perform a numerical 112
integration to account for the variation of the index of refraction with altitude 113
assuming that the emission travels in straight lines to the observer (see below). 114
The curvature of the Earth’s atmosphere is fully accounted for in AIRES. 115

We have modified the ZHAireS code to deal with the reflection of air shower 116
radio emission on a surface. For each rectilinear track element we first find 117
the point on the reflection surface and the angle of emission of radiation with 118
respect to the track so that the emitted ray propagates first to the reflection 119
point and then upwards towards the observer at a fixed position. Approximat- 120
ing the reflection surface to a plane makes it trivial to obtain this reflection 121
point for a ray coming from any point in the atmosphere. Once this is known, 122
the time delay due to the refractive index is easily calculated integrating the 123
travel time over the total path of the ray before and after the reflection. We 124
assume that the emission travels in a straight lines to the observer. We have 125
explored the validity of this approximation using a simple one dimensional 126
model to produce pulses which resemble the fully simulated ones. This model 127

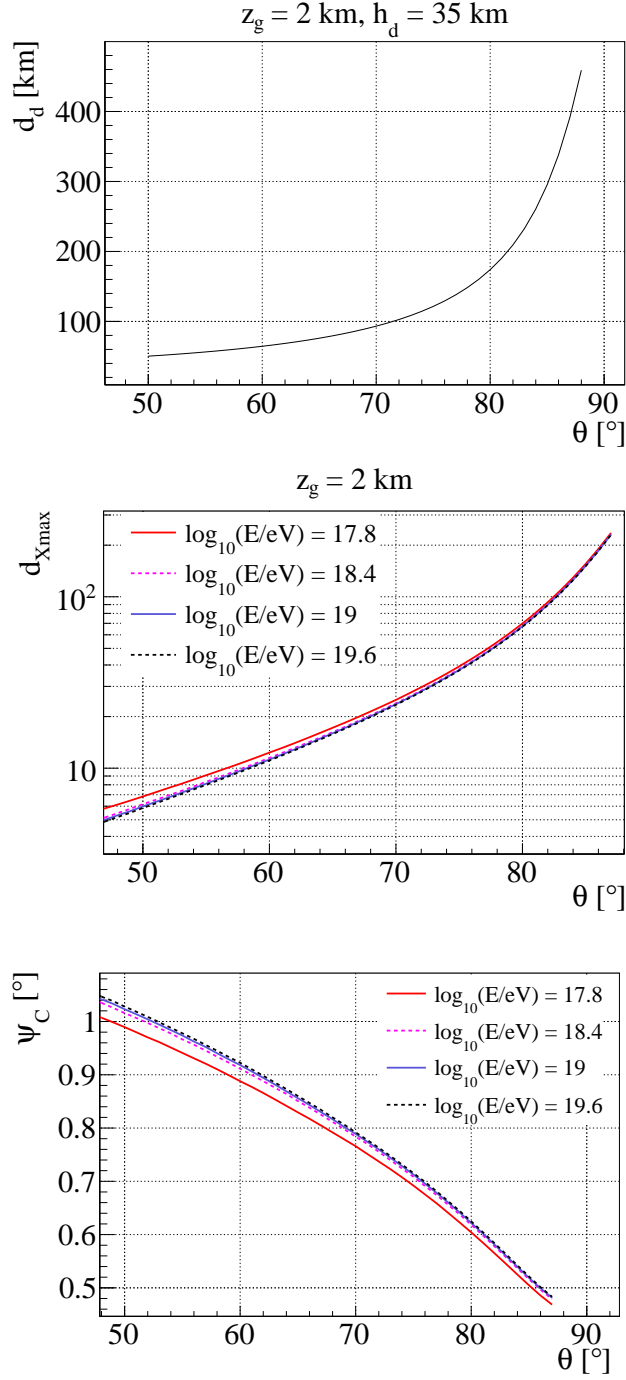


Fig. 3. Top panel: distance from the reflection point to the detector (d_d in Fig. 1); middle panel: distance to shower maximum ($d_{X_{\max}}$ in Fig. 1); and bottom panel: the Cherenkov angle at X_{\max} as a function of shower zenith angle. For the location of X_{\max} we used the average value of $\langle X_{\max} \rangle$ as a function of energy as measured by the Pierre Auger Collaboration [18,19].

allows the calculation of travel times using numerical methods to propagate signals along curved trajectories. The properties of the pulses obtained with straight ray approximation are equivalent to those accounting for curvature up to shower zenith angles $\theta \sim 85^\circ$ and frequencies of ~ 1 GHz. This study is described in detail in the Appendix.

As mentioned before, we approximate the reflection surface to the xy -plane defined in Section 2, assumed to be perfectly flat. The bulk of the emission has been shown to be concentrated in a cone that makes a small “off-axis” angle ψ to the shower direction as shown in Fig. 2. This angle is very close to the Cherenkov angle ($0.5^\circ - 1^\circ$) at an altitude at which shower maximum occurs [8]. As a consequence the illuminated region on the reflective surface is relatively small, of order $0.5 \text{ km} \times 1 \text{ km}$ ($1.5 \text{ km} \times 10 \text{ km}$) for a $\theta = 60^\circ$ (80°) shower. As a result it is reasonable to ignore the differences in the orientation angle and altitude of the reflecting surface at the locations of the different reflection points across the illuminated area. These differences are below 0.1° and a few meters respectively even for showers of $\theta = 80^\circ$. There are other important aspects to the flat mirror approximation. When rays are reflected on a convex and rough surface they will diverge after reflection, and therefore the power received at a given surface element will be typically less than when a flat reflector is assumed. These effects have been studied in [15] and [25], and have little impact at moderate zenith angles, however they can become significant for high zenith angles ($\theta > 80^\circ$). Results of the simulations with the reflective surface assumed flat can be corrected “a posteriori” following the procedures outlined in [15,25]. Such calculation is however very detector specific, and out of the scope of this article. Despite this, we expect the simulation method presented in this work to be very suitable for that purpose.

At each reflection point the Fresnel coefficients are applied to the time-domain electric field to calculate the attenuation of the components with polarization parallel, r_{\parallel} , and perpendicular, r_{\perp} , to the reflection plane, defined by the normal to the reflecting surface and the direction of the radiation:

$$r_{\perp} = \frac{n_1 \cos \theta - n_2 \sqrt{1 - \left(\frac{n_1}{n_2} \sin \theta\right)^2}}{n_1 \cos \theta + n_2 \sqrt{1 - \left(\frac{n_1}{n_2} \sin \theta\right)^2}}, \quad \text{and} \quad r_{\parallel} = \frac{n_1 \sqrt{1 - \left(\frac{n_1}{n_2} \sin \theta\right)^2} - n_2 \cos \theta}{n_1 \sqrt{1 - \left(\frac{n_1}{n_2} \sin \theta\right)^2} + n_2 \cos \theta}. \quad (1)$$

The Fresnel coefficients for an air-ice interface are shown in Fig. 4 as a function of zenith angle θ of the incident ray. A large fraction of the components of the field is not reflected below $\theta \sim 70^\circ - 80^\circ$, and in fact at the Brewster angle at $\theta \sim 53^\circ$ the parallel component is not reflected at all. The coefficients change rapidly above $\theta \sim 60^\circ$. Clearly they have a drastic impact on the overall amplitude, the polarization and the zenith angle dependence of the radio signal as will be shown in Section 4.

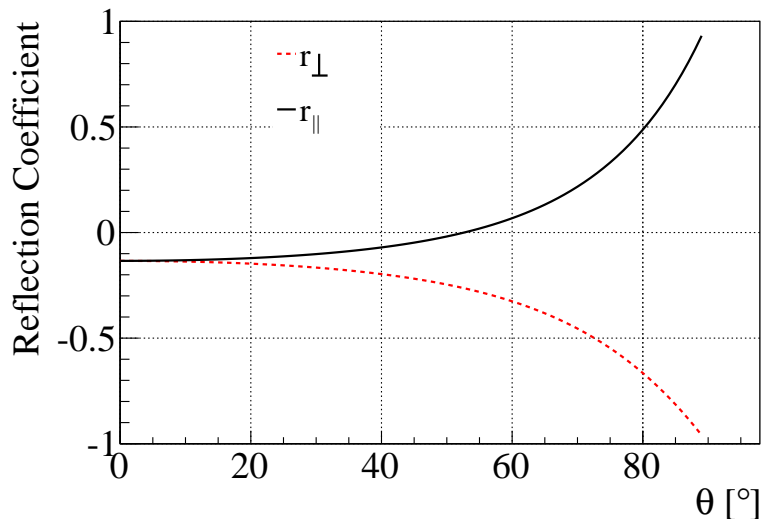


Fig. 4. The Fresnel coefficients for an air-ice interface with refractive indices 1.0003 and 1.31 respectively, as a function of the zenith angle θ of the incident ray.

161 4 Simulations for a high altitude detector

162 4.1 Simulation set and considerations

163 In this section we apply the implementation of the reflection in ZHAireS to a
 164 configuration that resembles a high altitude balloon experiment over Antarc-
 165 tica, such as the ANITA flights, or the planned EVA mission [14].

166 We place antennas at a fixed altitude $h_d = 36$ km above sea-level, and choose
 167 the reflecting surface to be at $z_g = 2$ km above sea-level. We adopt a refractive
 168 index of $n = 1.31$ [26] consistent with ANITA measurements of the reflected
 169 image of the Sun [27]. The geomagnetic field is chosen to have a typical value²
 170 of $55 \mu\text{T}$ and an inclination of -70° . We generated proton showers with zenith
 171 angles $\theta = \{57^\circ, 64^\circ, 71^\circ, 78^\circ, 85^\circ\}$ and azimuth such that they always arrive
 172 from the geomagnetic west. For each zenith angle, we generate air showers
 173 with energies $E = \{10^{17.8}, 10^{18.4}, 10^{19}, 10^{19.6}\}$ eV. We select simulations that
 174 have a X_{max} similar to the average $\langle X_{\text{max}} \rangle_{\text{Auger}}$ observed at the Pierre Auger
 175 Observatory. To do so, we pre-simulate seven air showers per configuration
 176 with different random seeds and we select the air shower closest to $\langle X_{\text{max}} \rangle_{\text{Auger}}$.
 177 This results in an average deviation of $|X_{\text{max}} - \langle X_{\text{max}} \rangle_{\text{Auger}}| \approx 18 \text{ g cm}^{-2}$, which
 178 is within the root mean square of the energy-dependent X_{max} -distributions
 179 that have been observed. The shower simulation is run with AIRES using
 180 QGSJETII.03 hadronic model interactions with a thinning level of 10^{-5} [20].

² See for example <http://www.ngdc.noaa.gov/geomag/geomag.shtml>

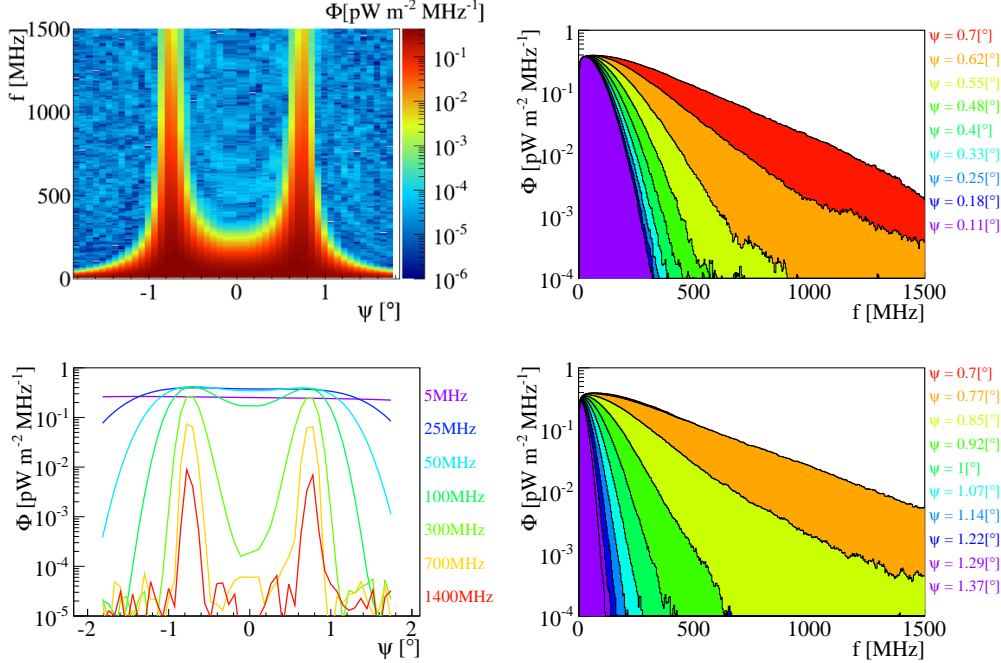


Fig. 5. Top left panel: distribution of the radio signal (flux density Φ) as a function of off-axis angle ψ (Fig. 2) and frequency f for an air shower with $\theta = 71^\circ$ and $\log_{10}(E/\text{eV}) = 18.4$. In the bottom left panel we show the distribution of the radio signal as a function of off-axis angle at various frequencies. In the right panels we show the radio signal distribution as a function of frequency, in the top right panel for off-axis angles equal or smaller than the Cherenkov-angle at the X_{max} of the shower i.e. $\psi \leq 0.7^\circ$, while in the bottom right panel for $\psi \geq 0.7^\circ$.

4.2 Results

181

To illustrate some of the typical features of the radio signal, we display in Fig. 5 182
the flux density Φ as a function of frequency and off-axis angle ψ for an air shower 183
with zenith angle $\theta = 71^\circ$ and a energy $E = 10^{17.8}$ eV. The flux density 184
in this case is defined as the power spectrum at a fixed frequency f averaged 185
over a period of 10 ns, and is given in units of $\text{pW m}^{-2} \text{MHz}^{-1}$ throughout 186
this paper. In the top left panel of Fig. 5 we show the two-dimensional distribu- 187
tion as a function of ψ and f which displays coherent properties and is 188
clearly beamed around the Cherenkov angle at $\sim 0.77^\circ$. This can be better 189
appreciated in the bottom left panel where we show the off-axis distributions 190
for different frequency components of the pulse. As the frequency increases 191
the radiation adds coherently only within a smaller angle off the Cherenkov 192
cone. In the right panels in Fig. 5 we show the spectral shape of the flux 193
density for a variety of observation off-axis angles. At very low frequencies 194
($f < 10$ MHz) the flux density increases until it reaches a maximum in the 195
range ($f \sim 10 - 150$ MHz) and then decreases with an exponential fall-off 196
to first order. A very important feature is illustrated in the right panels, the 197

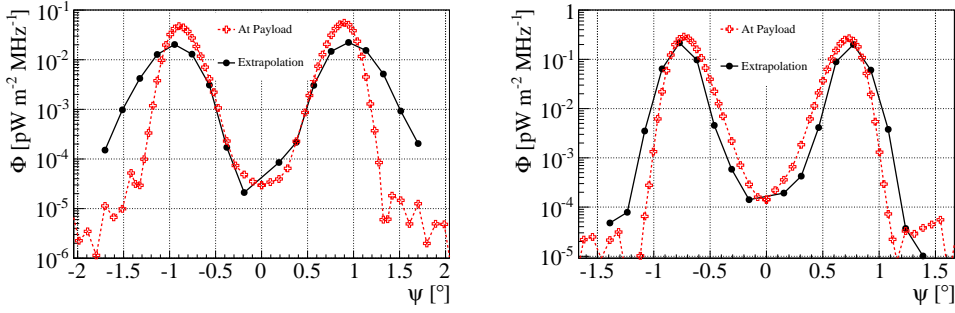


Fig. 6. Flux density Φ at a frequency $f = 300$ MHz as a function of off-axis angle ψ as obtained extrapolating the ZHAireS simulated signal at ground to the detector (black dots and solid line), and simulating the reflection as explained in the text (red crosses and dashed line). The flux density is shown for showers of $E = 10^{18.4}$ eV and two zenith angles $\theta = 57^\circ$ (left panel) and $\theta = 71^\circ$ (right panel). The Fresnel-reflection coefficients are accounted for in all cases.

198 steepness of the fall-off has a clear dependence on the off-axis angle ψ of the
 199 detector. This dependence is key to the energy determination of UHECRs with
 200 ANITA as pointed out in [28].

201 4.2.1 Implications of the reflection

202 Other efforts to simulate reflected radio signals from air showers have relied on
 203 pulses simulated at ground which were extrapolated using the attenuation of
 204 the signal with increased distance ($|\vec{E}| \propto 1/r$) after accounting for the loss of
 205 signal induced by the Fresnel coefficients [28]. In a homogeneous medium this
 206 “specular approach” can be expected to be a good approximation provided
 207 the pulse can be considered to be in the Fraunhofer limit. As a result it can be
 208 expected to work better for highly inclined showers, since the distance between
 209 the observer and air shower increases as the zenith angle rises.

210 In this work all track contributions to the pulse are reflected at the interface
 211 to account for attenuation with distance, for the Fresnel-reflection coefficients
 212 attenuating the parallel and perpendicular components of the field, and for
 213 the fact that reflection also alters the relative time delays of emission from
 214 different regions of the shower affecting the coherence properties of the pulses.
 215 Therefore, this method can also be applied when the reflector is not in the
 216 Fraunhofer limit.

217 We compare the specular approximation to the results of the full ZHAireS
 218 simulation including reflection to illustrate the difference between the two
 219 methods. For this comparison we evaluate the flux density at $f = 300$ MHz
 220 at a few ground locations scaling it to account for the distance from ground
 221 to the location of the high altitude balloon. In Fig. 6 we display the flux
 222 density as a function of ψ for two different zenith angles. We note that for

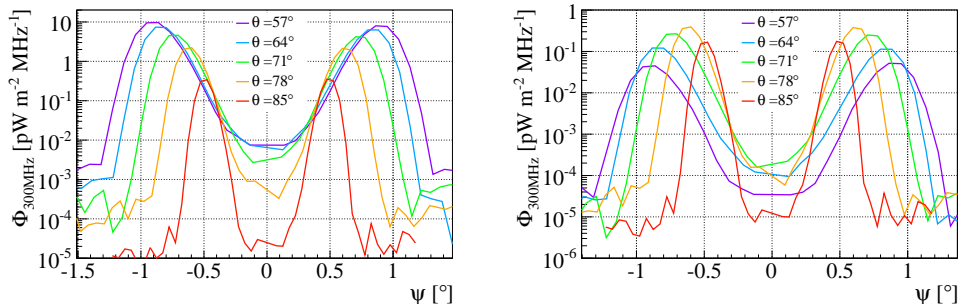


Fig. 7. Comparison of the flux density Φ at a frequency $f = 300$ MHz as a function of the off-axis angle ψ before (left) and after applying Fresnel reflection coefficients (right). Different sets of curves correspond to different shower zenith angles θ as labeled. The simulated showers have an energy $E = 10^{18.4}$ eV.

$\theta = 57^\circ$ (Fig. 6 left) the distribution in ψ is significantly wider what can lead to orders of magnitude of over-estimation of the flux density for the larger off-axis angles. For $\theta = 71^\circ$ (Fig. 6 right) we still see relevant deviations between the two methods, but they are significantly reduced compared to the lower zenith angle case. Significant deviations are also found at other frequencies. Moreover, the shapes of the frequency spectra obtained with the two methods also differ appreciably.

It is interesting to explore how the radiation changes with zenith angle for a primary particle with fixed energy. As the zenith angle increases the flux density Φ decreases. This can be seen in the left panel of Fig. 7, displaying Φ at $f = 300$ MHz as a function of ψ for an air shower induced by a primary particle with energy $E = 10^{18.4}$ eV. The dominant effect in the decrease is the increasing overall distance to the detector with θ (see Fig. 3). Other effects however compensate the decrease in Φ . The angle α of the shower axis to the Earth's magnetic field at the South Pole increases in the range of θ shown in Fig. 7, and the geomagnetic contribution is known to scale with $\sin \alpha$. Also showers of increasing θ develop in a less dense atmosphere where the geomagnetic contribution to the electric field is expected to be increasingly larger [30]. The net result, including other more subtle effects [29], is a decrease of Φ with θ .

To illustrate the importance of accounting for the Fresnel reflection coefficients they were artificially set to 1 in the simulations shown in the left panel of Fig. 7, while in the right panel they are taken into account. Comparing both panels, the peak value of the flux density is largest at relatively high zenith angles ($\theta \sim 80^\circ$) when the Fresnel coefficients are accounted for, contrary to what is seen in the left panel where the peak value of Φ is achieved at the smallest zenith angles. This suggests that detection can be expected to be most favorable for θ around 80° . A thorough calculation of the acceptance integrating over area and solid angle [13] should also account for the reduction

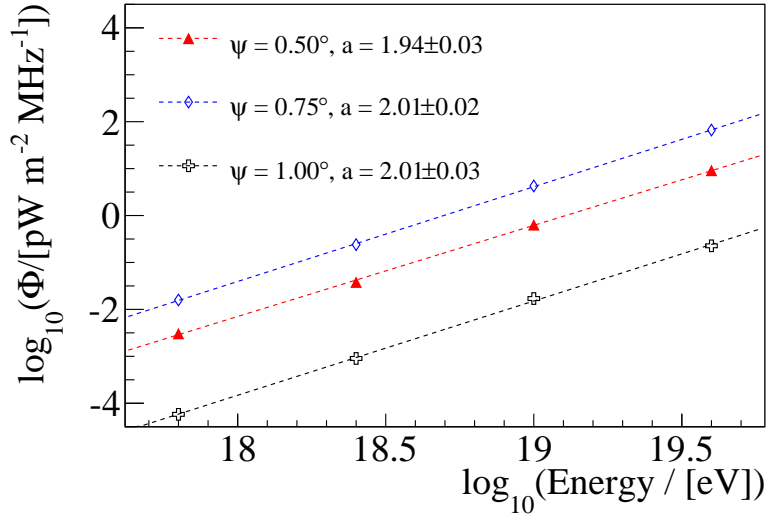


Fig. 8. The flux density Φ at frequency $f = 300$ MHz as a function of the energy of the primary particle for three off-axis angles in a shower of $\theta = 71^\circ$. The results of fitting a straight line $\log_{10} \Phi = a \log_{10}(E/\text{eV}) + b$ are shown.

252 of the Cherenkov angle as the zenith angle rises (see Fig. 3), and for the
 253 directionality of the detection system. Such calculation is out of the scope of
 254 this article.

255 4.2.2 Energy dependence

256 From the set of simulations we have examined the energy dependence of the
 257 radio signal. As before, we use the flux density at a reference frequency $f =$
 258 300 MHz for a shower of $\theta = 71^\circ$.

259 In Fig. 8 we select three off-axis angles and plot the flux density as a function of
 260 the primary particle energy. We fit a simple linear function to the dependence
 261 of $\log_{10} \Phi$ on $\log_{10}(E)$ and find a slope that is consistent with 2. This confirms
 262 that the received flux density scales quadratically with the primary energy and
 263 the amplitude of the electric field scales linearly with it. This is not surprising
 264 since for a coherent signal it is expected that the amplitude of the electric
 265 field scales with the number of electrons in the shower which is proportional
 266 to the energy of the primary particle. We verified that the quadratic relation
 267 between flux density and energy of primary cosmic ray particle holds for all
 268 the zenith angles and all considered frequencies in our simulation set. This
 269 has important consequences since measuring the flux density at a given off-
 270 axis angle provides a measurement of the energy of the air shower. In practice
 271 the off-axis angle can be related to the exponential fall-off of the flux density
 272 as can be seen in Fig. 5. This relation is key to the energy determination
 273 of UHECRs with ANITA [28]. This means that it is in principle possible to

deduce the primary energy from a single location as long as the exponential
fall-off of the spectrum can be determined.

5 Conclusions

In this paper we implemented the treatment of surface reflection for radio
signals from air showers, upgrading existing ZHAireS simulations³.

As a case study we simulated radiation from a set of air showers at a high
altitude position over Antarctica inspired by the ANITA experiment which has
provided the only measurements of reflected radio pulses from air showers up to
now. We described and explained the flux density distributions as a function of
frequency, energy and zenith angle of the primary cosmic ray particle. We have
stressed the importance of accounting for the Fresnel-reflection coefficients
attenuating the components of the field, as well as accounting for the fact
that reflection also alters the relative time delays of emission from different
regions of the shower affecting the coherence properties of the pulses.

A clear quadratic correlation between the radio observable (flux density) and
the shower energy has been observed in ZHAireS simulations with reflection.
The intercept of the correlation depends on the off-axis angle which can be
related to the exponential fall-off of the spectral distribution of the flux density.
This provides the basis for the determination of shower energy from a single
location [28].

Several approximations were made in the implementation of the reflection in
the ZHAireS code. The reflective surface is assumed to be a plane and we
argued that this is a good approximation as long as the shower zenith angle
is $\theta \lesssim 80^\circ$. Also the emitted radiation is assumed to travel along straight
lines to the ground and then to the detector, an approximation that has been
extensively verified in Appendix A.

Finally, we foresee many applications of this code to the design and feasibil-
ity studies of future large exposure cosmic ray detectors based on the radio
technique applied to air showers [15,13].

³ Code available upon request.

303 Acknowledgements

304 We thank Ministerio de Economía (FPA2012-39489), Consolider-Ingenio 2010
305 CPAN Programme (CSD2007-00042), Xunta de Galicia (GRC2013-024), Feder
306 Funds and Marie Curie-IRSES/ EPLANET (European Particle physics Latin
307 American NETwork), 7th Framework Program (PIRSSES- 2009-GA-246806).
308 H.S. is supported by Office of Science, U.S. Department of Energy and N.A.S.A.
309 We also thank CESGA (Centro de Supercomputación de Galicia) for comput-
310 ing resources.

311 References

- 312 [1] D. Ardouin *et al.* [CODALEMA Collaboration], *Astropart. Phys.* **31** (2009)
313 192.
- 314 [2] P. Schellart *et al.* [LOFAR Collaboration], *Astron. & Astrophys.* **560** (2013)
315 A98.
- 316 [3] F.G. Schröder for the Pierre Auger Collaboration, Proceedings of the 33rd
317 ICRC, Rio de Janeiro, Brazil (2013), #0899.
- 318 [4] H. Falcke *et al.* [LOPES Collaboration], *Nature* **435** (2005) 313.
- 319 [5] F.G. Schröder for the Tunka-Rex Collaboration, Proceedings of the 33rd ICRC,
320 Rio de Janeiro, Brazil (2013), #0452.
- 321 [6] T. Huege, Proceedings of the 33rd ICRC, Rio de Janeiro, Brazil (2013), *Braz.*
322 *J. Phys.* **44** (2014) 520, also available as arXiv:1310.6927 [astro-ph].
- 323 [7] R. Šmída *et al.* [CROME collaboration], *Phys. Rev. Lett.* **113** (2014) 221101
- 324 [8] J. Alvarez-Muñiz, W.R. Carvalho, A. Romero-Wolf, M. Tueros and E. Zas,
325 *Phys. Rev. D* **86** (2012) 123007
- 326 [9] S. Hoover *et al.*, *Phys. Rev. Lett.* **105** (2010) 151001.
- 327 [10] F.D Kahn, I. Lerche, *Proc. R. Soc. Lond. A* **289**, 1417 (1966) 206
- 328 [11] F. Halzen, E. Zas, T. Stanev, *Phys. Lett. B* **257** (1991) 432.
- 329 [12] J. Alvarez-Muñiz, R.A. Vázquez and E. Zas, *Phys. Rev. D* **61** (1999) 023001.
- 330 [13] P. Motloch, N. Hollon, P. Privitera, *Astropart. Phys.* **54** (2014) 40.
- 331 [14] P. W. Gorham, *et al.* *Astropart. Phys.* **35** (2011) 242.
- 332 [15] A. Romero-Wolf *et al.*, arXiv:1302.1263 [astro-ph].
- 333 [16] J. Alvarez-Muñiz, W.R. Carvalho and E. Zas, *Astropart. Phys.*, **35**, 325, (2012).

- [17] J. Alvarez-Muñiz, R.A. Vázquez and E. Zas, Phys. Rev. D **62** (2000) 063001. 334
- [18] P. Abreu *et al.* [The Pierre Auger Collaboration], Phys. Rev. Lett. **104** (2010) 091101. 335
336
- [19] A. Aab *et al.* [The Pierre Auger Collaboration], arXiv1409.4809 [astro-ph]. 337
- [20] S. J. Sciutto, arXiv 99.11.331, (1999), 338
<http://www2.fisica.unlp.edu.ar/auger/aires>. 339
- [21] E. Zas, F. Halzen, T. Stanev, Phys. Rev. D **45**, 362 (1992). 340
- [22] J. Alvarez-Muñiz, A. Romero-Wolf, E. Zas, Phys. Rev. D **81** (2010) 123009. 341
- [23] D. García-Fernández, J. Alvarez-Muñiz, W.R. Carvalho, A. Romero-Wolf and 342
E. Zas, Phys. Rev. D **87** (2013) 023003. 343
- [24] J. Alvarez-Muñiz, A. Romero-Wolf, E. Zas, Phys. Rev. D **81** (2010) 123009. 344
- [25] A. Romero-Wolf, S. Vance, F. Maiwald, E. Heggy, P. Ries, K. Liewer, 345
arXiv:1404.1876 [astro-ph]. 346
- [26] I. Kravchenko, D. Besson, J. Meyers, Journal of Glaciology, **50** (2004) 171. 347
- [27] D. Z. Besson, *et al.* Radio Science (in press) arXiv:1301.4423 [astro-ph]. 348
- [28] K. Belov for the ANITA collaboration, AIP Conf. Proc. **1535** (2013) 209. 349
- [29] J. Alvarez-Muñiz, W.R. Carvalho Jr., A. Romero-Wolf, M. Tueros, E. Zas, AIP 350
Conf. Proc. **1535** (2013) 143. 351
- [30] O. Scholten, K. Werner, F. Rusdyi, Astropart. Phys. **29** (2008) 94. 352
- [31] K. Werner, O. Scholten, Astropart. Phys. **29** (2008) 393. 353

A Appendix 354

A.1 Straight vs curved ray propagation 355

The variation with altitude of the index of refraction of the atmosphere is 356
known to induce curvature in the path of the radio waves when propagating. 357
It has been shown that the effects are negligible for most shower geometries 358
and observers on ground [31], for which the propagation along straight paths 359
is a good approximation. In the case of showers at large zenith angles and 360
especially when accounting for reflection, the involved distances from emission 361
to the detector become large (see Figs. 1 and 3), and the curvature of the rays 362
can be expected to increase. 363

364 To evaluate if the approximation of straight light ray propagation still holds in
 365 the typical geometries involved in reflection, we have developed a simple ray
 366 tracing code. We divide the atmosphere in many layers with constant distance
 367 between them. The layers are taken sufficiently narrow so that the ray can be
 368 approximated as traveling in a straight line along a constant refractive index n
 369 in each layer given by the exponential model in Section 2. The ray is refracted
 370 at each interface, taking into account the different refractive index at each
 371 layer. The travel time of the ray is calculated as the sum of the times it takes
 372 to cross each layer. When accounting for reflection on the ground, the ray is
 373 also propagated upwards through a decreasing refractive index profile until it
 374 reaches the detector. The arrival time assuming straight line propagation to
 375 ground and then to the same detector position is also calculated. The reflection
 376 surface is assumed to be at sea level for these calculations. Since the gradient
 377 of an exponential atmosphere is largest at sea level, it can be expected that
 378 curvature effects for reflection from surfaces at higher altitudes will have less
 379 impact than estimated here.

380 In Fig. A.1 (top panel) we show the relative arrival times of radio signals
 381 emitted from different positions along the shower axis of a $\theta = 70^\circ$ shower.
 382 They have been calculated with the straight and curved ray approximations
 383 for two particular observer positions such that the radiation arriving from
 384 shower maximum makes an off-axis angle $\psi \sim 0.77^\circ$. One observer is located
 385 on the ground and receives the rays directly, the other observer is placed at
 386 an altitude $h_d \simeq 33$ km and receives the rays after reflection on the ground
 387 (see Fig. 1). The difference in the arrival times between curved and straight
 388 ray propagation is hardly noticeable in the scale of Fig. A.1. It is in fact
 389 below ~ 50 ps, which corresponds to a frequency of ~ 5 GHz when using a
 390 quarter wavelength criterion for coherence. As a result we expect the straight
 391 ray approximation to be valid below this frequency.

392 Similarly in Fig. A.1 (bottom panel) we show the arrival times of the pulses
 393 for a $\theta = 85^\circ$ shower and observation at an off-axis angle $\psi = 0.4^\circ$. Although
 394 in this case the difference between curved and straight ray propagation is
 395 sizable, it is an almost constant offset along shower development of ~ 0.3
 396 ns for the observer on the ground and ~ 0.9 ns for the observer at high
 397 altitude $h_d = 50$ km. This global offsets induce unobservable phase shifts
 398 in the field at the detector. When accounting for these offsets, the relative
 399 differences between the straight and curved propagations are ~ 200 ps for the
 400 observer at ground level corresponding to a frequency of ~ 1.25 GHz using a
 401 quarter wavelength criterion, while for the observer at $h_d = 50$ km altitude
 402 the differences are below ~ 20 ps (~ 12 GHz frequency).

403 In the top and bottom panels of Fig. A.1 the relative arrival times at ground
 404 and at the high altitude observer are approximately flat within a large region
 405 (~ 10 km) around shower maximum. As a result the emission from this region

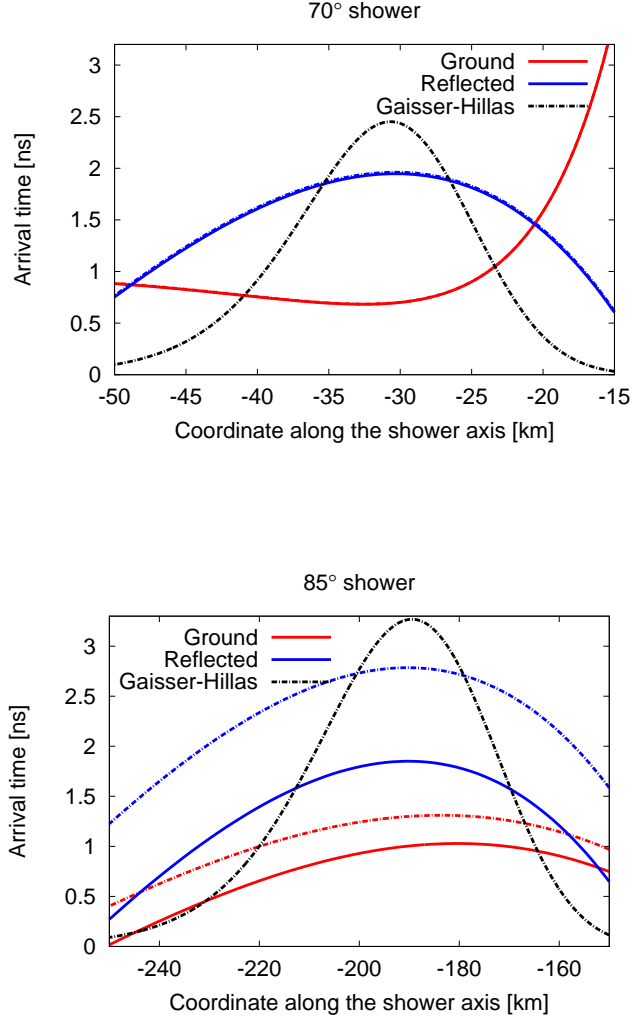


Fig. A.1. Top: Relative arrival time of rays emitted along the axis of a $\theta = 70^\circ$ shower at two particular antenna locations: one located on the ground (red lines) and another after reflection towards a high altitude balloon (blue lines) both at an off-axis angle close to the Cherenkov angle $\psi \sim 0.77^\circ$ (see Fig. 2). The straight ray approximation (dashed lines) and the curved ray propagation (solid lines) are shown (see text for details). A 10^{19} eV, $\theta = 70^\circ$ Gaisser-Hillas shower profile is superimposed (black line). Bottom: the same as in the top panel, but now for a $\theta = 85^\circ$ shower viewed at an off-axis angle $\psi \sim 0.40^\circ$.

is coherent up to GHz frequencies. An interesting feature in the top panel 406
of Fig. A.1 is the inversion of the arrival times at the high altitude observer 407
position. The radio signal emitted in the Cherenkov angle (in this particular 408
case from the region around shower maximum) arrives last at the high altitude 409
location, contrary to what could be expected in a homogeneous medium. The 410
time inversion is also seen for the observer on the ground for the 85° shower 411

412 in Fig. A.1 (bottom). The effect does not seem to have relevant implications
 413 for detection.

414 *A.2 A simple model to describe the pulses*

415 The comparison of the travel times for the straight and curved ray calculations
 416 already sheds light onto the validity of the straight ray approximation. How-
 417 ever a comparison between the pulses obtained with the straight and curved
 418 approaches in a simplified calculation will give us an estimate of the quanti-
 419 tative uncertainty in the properties of the signal at the detector when using
 420 the straight path approximation.

For that purpose, we model a shower with zenith angle θ as a one-dimensional charge distribution varying with time $N(t)$ as the shower propagates along a given direction at the speed of light c [17]. In the Fraunhofer approximation [23], the electric field induced by this line of charge is proportional to the charge $N(t)$, to $r^{-1}(t)$, with $r(t)$ the distance between the emission point and the observer position, and carries a phase factor to account for the time delay between the arrival of the signal emitted from different positions along the line:

$$E \sim \int dt N(t) \frac{e^{i\omega t_a(t)}}{r(t)} \quad (\text{A.1})$$

Here ω is the angular frequency and t_a is the arrival time at the observer of a signal emitted at time t , where

$$t_a(t) = t + \frac{n}{c} r(t) \quad (\text{A.2})$$

421 This approximation was developed for a homogeneous, isotropic and non-
 422 conductive medium but it can be extended to the atmosphere accounting for
 423 the time delays from propagation of the rays in the altitude-dependent index
 424 of refraction [16].

425 In Fig. A.2 the pulses obtained in the full ZHAireS simulation modified for
 426 reflection are compared to those obtained with Eq. (A.1) using as input a one-
 427 dimensional Gaisser-Hillas distribution, $N(t)$, with the same depth of shower
 428 maximum as the simulated shower. The amplitude of the reflected field is
 429 shown for observers at a high altitude located at different off-axis angles ψ (see
 430 Fig. 2) and constant overall path distance. The results have been normalized
 431 to the peak of the electric field as predicted with Eq. (A.1). The shape of the
 432 angular distribution is well described by the simple model in a wide frequency
 433 range. It should be noted here that, being one-dimensional, the approach can
 434 not fully reproduce the frequency spectrum as obtained in the full simulations
 435 near the Cherenkov angle, where the lateral spread is of utmost importance

[16]. We are however confident that the approximation is sufficient to test the validity of the straight ray approximation. 436
437

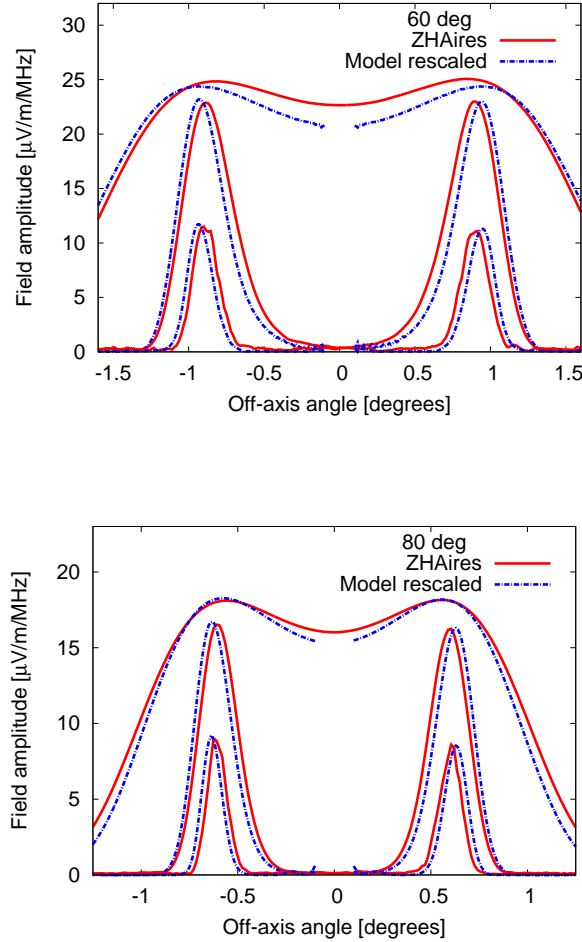


Fig. A.2. Top: amplitude of the Fourier transformed electric field as a function of the off-axis angle for different frequencies. Results from full ZHAireS simulations and the model in Eq. (A.1) are shown. The shower has $E = 10^{19}$ eV, $\theta = 60^\circ$ and a height of X_{max} above ground $h_{X_{\text{max}}} \sim 4.4$ km. The observers are placed at a constant distance from X_{max} of ~ 83.3 km. From top to bottom the observation frequencies are 50, 300 and 900 MHz. Bottom: Same as in the top panel, but for a $\theta = 80^\circ$ shower with $h_{X_{\text{max}}} \sim 13.5$ km and with the observers placed at a constant distance of ~ 276.9 km.

A.3 Validity of the straight ray approximation 438

We used the simplified one-dimensional model described above to test the straight ray approximation. The arrival times t_a at the detector to be used in Eq. (A.1) are calculated integrating the travel time along both straight and 439
440
441

442 curved paths using the ray tracing algorithm explained above. The electric field
443 is obtained numerically, discretizing the integral in Eq. (A.1) in such a way
444 that the time intervals correspond to regions of the shower with approximately
445 constant $N(t)$, $r(t)$ and $t_a(t)$.

446 The results using the straight and curved ray calculations are compared in
447 Fig. A.3 where we plot the modulus of the electric field as a function of the
448 offset angle of the antenna ψ for showers of $\theta = 70^\circ$ (top) and $\theta = 85^\circ$
449 (bottom). As anticipated from arguments concerning the travel times discussed
450 at the beginning of this Appendix, the difference in the angular distribution of
451 the electric field between the straight and curved ray propagation is negligible
452 for the $\theta = 70^\circ$ shower at all the frequencies we probed. It can be appreciated
453 that even for $\theta = 85^\circ$, the effect is still negligible up to a frequency of 900 MHz.
454 This justifies the straight ray approximation for the calculation of the angular
455 distribution of the field, even at high zenith angles and up to GHz frequencies.

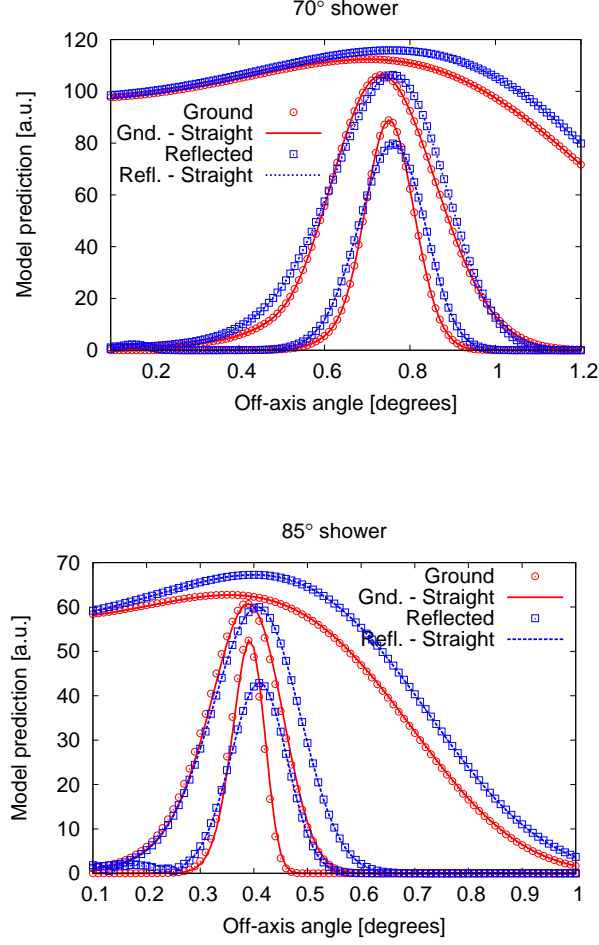


Fig. A.3. Top: Electric field modulus as obtained with the simple model in Eq. (A.1), as a function of the off-axis angle ψ for three frequencies. The observers are located at different ψ angles on the ground (red solid lines) and at an overall distance ~ 130 km to X_{\max} after reflection (blue dashed lines). The shower has $\theta = 70^\circ$ and X_{\max} at an altitude above ground $h_{X_{\max}} \sim 10.4$ km. The results of curved (points) and straight (lines) rays calculation are shown. From top to bottom, the observation frequencies are 50, 300 and 900 MHz. Bottom: the same as in the top panel with the observers located on the ground and at an overall path distance of ~ 648.5 km. The shower has $\theta = 85^\circ$ and $h_{X_{\max}} \sim 16.5$ km. In both panels the fields on the ground are rescaled with the corresponding ratio of the distance to the ground and the total distance to the detector for visibility.